

Effect of zirconia on improving NO_x reduction efficiency of Nd₂Zr₂O₇ nanostructure fabricated by a new, facile and green sonochemical approach

Sahar Zinatloo-Ajabshir^{a,*}, Naser Ghasemian^a, Mehdi Mousavi-Kamazani^b, Masoud Salavati-Niasari^c

^a Department of Chemical Engineering, University of Bonab, P.O. Box. 5551761167, Bonab, Iran

^b New Technology Faculty, Semnan University, Semnan, Iran

^c Institute of Nano Science and Nano Technology, University of Kashan, Kashan, P. O. Box. 87317-51167, Iran

ARTICLE INFO

Keywords:

Nd₂Zr₂O₇
Ceramic
Sonochemistry
Propane-SCR
NO_x reduction

ABSTRACT

Here, we offer an easy and eco-friendly sonochemical pathway to fabricate Nd₂Zr₂O₇ nanostructures and nanocomposites with the help of *Morus nigra* extract as a new kind of capping agent. For the first time, the performance of Nd₂Zr₂O₇-based ceramic nanostructure materials has been compared upon NO_x abatement. Diverse kinds of techniques have been employed to specify purity and check the attributes of the fabricated Nd₂Zr₂O₇-based nanostructures by *Morus nigra* extract. Outcomes revealed the successful fabrication of Nd₂Zr₂O₇ nanostructures and nanocomposites applying *Morus nigra* extract through sonochemical pathway. All nanostructured samples have been fabricated through ultrasonic probe with power of 60 W (18 KHz). Further, the fabricated Nd₂Zr₂O₇-based ceramic nanostructure materials can be applied as potential nanocatalysts with appropriate performance for propane-SCR-NO_x, since the conversion of NO_x to N₂ for the best sample (Nd₂Zr₂O₇-ZrO₂ nanocomposite) was 70%. In addition, in case of Nd₂Zr₂O₇-ZrO₂ nanocomposite, the outlet quantity of CO as an unfavorable and unavoidable product was lower than the rest.

1. Introduction

Nowadays, the usage of nanoscale compounds in diverse fields is very significant [1–4]. Among the nanoscale compounds, rare earth zirconium oxides (Re₂Zr₂O₇) have been examined by the scholars because of their extraordinary attributes. These compounds are technologically a very beneficial kind of materials because of their usages in gas turbines [5], catalytic process [6–8], diesel engines [9], environmental remediation [10,11] and coating materials [12]. To date, a variety of approaches for making the nanostructured Re₂Zr₂O₇ has been offered and employed like combination of the sol–gel and coprecipitation [13], floating zone technique [14], solid-state reaction [6,15], microwave plasma technique [16] and Pechini approach [17]. Use of ultrasonic approach for making the nanoscale compounds, has fascinated extraordinary attention for its ease, fastness and low cost as well as its environmental friendliness [18–21]. Thus, many scientists have been tried to create a variety of nano compounds with the help of ultrasonic path [22,23]. Multiple bubbles are created within the sonochemical path. After growth stage, these bubbles destructed because of

the shake waves. The energy release by bubbles destruction can be reason to drive the chemical reactions to form the nano-compound [24,25]. There is no report about fabrication of Nd₂Zr₂O₇ nanostructures and nanocomposites through a simple and eco-friendly sonochemical pathway.

Chemical and physical attribute and efficiency of the nanoscale compounds can be dependent to fabrication path, size distribution, purity rate, shape of them [26–30]. To date, intense research attempt has been undertaken to adjust size distribution, purity rate, shape of the nanoscale compounds [31,32].

In recent times, multitude literatures have been published upon process of SCR-NO_x utilizing a variety of hydrocarbon compounds like propane [33,34] and also methane [35] as well as ammoniac in role of reductant. A variety of oxide compounds and also zeolites have been offered in the role of catalyst for NO_x abatement. These consist aluminum oxide (Al₂O₃), cerium oxide (CeO₂), zirconium oxide (ZrO₂), vanadium oxide (V₂O₅) as well as zeolites like ZSM-5 and clinoptilolite [36]. Ghasemian et al. introduced ion-exchanged clinoptilolite zeolite upon propane-SCR-NO_x [37]. Our research group examined the usage of

* Corresponding author.

E-mail address: s.zinatloo@ubonab.ac.ir (S. Zinatloo-Ajabshir).

<https://doi.org/10.1016/j.ultsonch.2020.105376>

Received 26 August 2020; Received in revised form 13 October 2020; Accepted 18 October 2020

Available online 23 October 2020

1350-4177/© 2020 The Authors.

Published by Elsevier B.V. This is an open access article under the CC BY-NC-ND license

(<http://creativecommons.org/licenses/by-nc-nd/4.0/>).

Table 1
Synthesis conditions for $\text{Nd}_2\text{Zr}_2\text{O}_7$ -based nanostructure materials.

| Sample no | Capping agent | Sonication (time-power) | Zr: Nd | Crystalline size (XRD/nm) | Figure of FESEM images |
|-----------|---------------------|-------------------------|--------|---------------------------|------------------------|
| 1 | Morus nigra extract | 10 min- 60 W | 1:1 | 11 | 4a and b |
| 2 | Morus nigra extract | 10 min- 60 W | 2:1 | 13.4 | 4c and d |
| 3 | Morus nigra extract | 10 min- 60 W | 1:2 | 15.5 | 4e and f |

$\text{Ln}_2\text{Zr}_2\text{O}_7$ ($\text{Ln} = \text{Nd}, \text{Pr}$) ceramics in role of catalytic materials to eliminate NO_x [38].

This paper offered novel framework and easy path to fabricate $\text{Nd}_2\text{Zr}_2\text{O}_7$ nanostructures with the help of ultrasonic approach. The study demonstrates the first try on checking the role of Morus nigra extract, as an eco-friendly kind of capping agent, in the sonochemical synthesis of $\text{Nd}_2\text{Zr}_2\text{O}_7$ nanostructures. Morus nigra extract has been utilized as a new kind of capping agent because it comprises high quantity of anthocyanins [39]. As-fabricated $\text{Nd}_2\text{Zr}_2\text{O}_7$ nanostructure has been employed as a potential nanocatalyst for NO_x abatement and its yield has been checked. The synthesis method has been demonstrated to have notable impact on attribute and performance of nanoscale compounds [24]. In our previous work, $\text{Nd}_2\text{Zr}_2\text{O}_7$ sample produced via combustion path and checked its performance on NO_x abatement [38]. Here, to examine the role of synthesis pathway, the activity of $\text{Nd}_2\text{Zr}_2\text{O}_7$ samples produced by two different pathways (sonochemical and combustion) on propane-SCR- NO_x is compared. In addition, the nanostructured $\text{Nd}_2\text{Zr}_2\text{O}_7\text{-ZrO}_2$ and $\text{Nd}_2\text{Zr}_2\text{O}_7\text{-Nd}_2\text{O}_3$ have been fabricated with the help of Morus nigra extract via sonochemical pathway, to check the possibility of coupling ZrO_2 or Nd_2O_3 into neodymium zirconate and its effect on shape, dimension and activity. So far, there is no report comparing the performance of $\text{Nd}_2\text{Zr}_2\text{O}_7$ -based ceramic nanostructure

materials (sonochemically fabricated by Morus nigra extract) on propane-SCR- NO_x . The outcomes signify that $\text{Nd}_2\text{Zr}_2\text{O}_7$ -based ceramic nanostructure materials (sonochemically fabricated by Morus nigra extract) may be applied as nanocatalysts with appropriate performance for propane-SCR- NO_x .

2. Experimental

2.1. Substances and characterization

Neodymium nitrate, diethylenetriamine (dien) and also zirconyl nitrate with analytical grade in fabrication of $\text{Nd}_2\text{Zr}_2\text{O}_7$ -based nanostructure materials have been applied without additional purification. The shape and dimension of $\text{Nd}_2\text{Zr}_2\text{O}_7$ -based nanostructure materials have been checked by a microscope (MIRA3 FEG-SEM). $\text{Nd}_2\text{Zr}_2\text{O}_7$ -based nanostructure materials have been scanned by X-ray diffractometer (Philips Company) to illustrate and verify the phase composition. The surface properties of $\text{Nd}_2\text{Zr}_2\text{O}_7$ -based nanostructure material have been checked with a nitrogen adsorption in a Micromeritics Tristar 3000 apparatus. FTIR studies on $\text{Nd}_2\text{Zr}_2\text{O}_7$ -based nanostructure materials have been accomplished applying a Magna-IR, spectrometer 550 Nicolet. TEM data for $\text{Nd}_2\text{Zr}_2\text{O}_7$ -based nanostructure materials have been recorded with a microscope (TEM, JEM-2100). All experiments have been conducted with a probe as ultrasound source. Its power has been regulated in 60 W.

2.2. Fabrication of $\text{Nd}_2\text{Zr}_2\text{O}_7$ -based nanostructures

$\text{Nd}_2\text{Zr}_2\text{O}_7$ nanostructures have been fabricated through a simple and eco-friendly sonochemical pathway in which Morus nigra extract has been applied as a new kind of capping agent. First, 5 ml of Morus nigra extract (Mn Ex) has been admixed to a solution mixture of neodymium nitrate and zirconyl nitrate (molar ratio of $\text{Zr}:\text{Nd} = 1:1$) under sonication (60 W). While the prepared mixture was subjected under ultrasound, a new precipitator namely diethylenetriamine (dien) was added drop by drop to the above mixture to achieve its pH to 6. The sonication

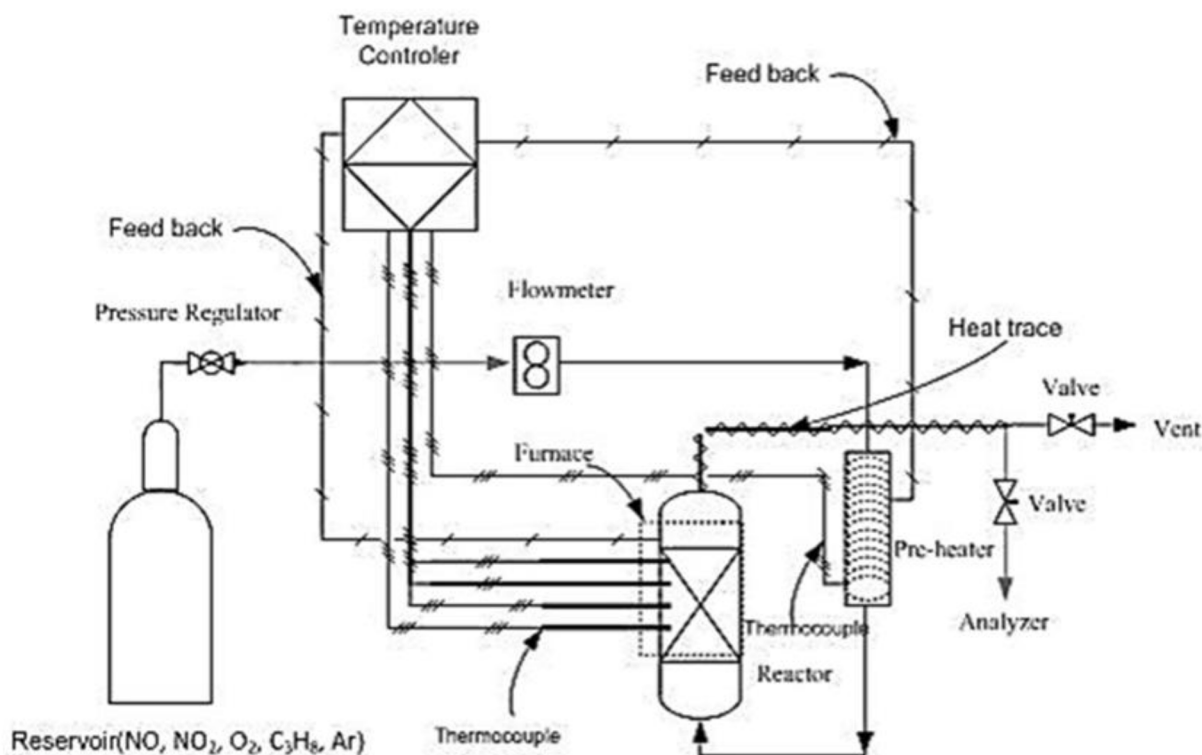


Fig. 1. Schematic illustration of integral catalytic reactor system for SCR- NO_x process [38].

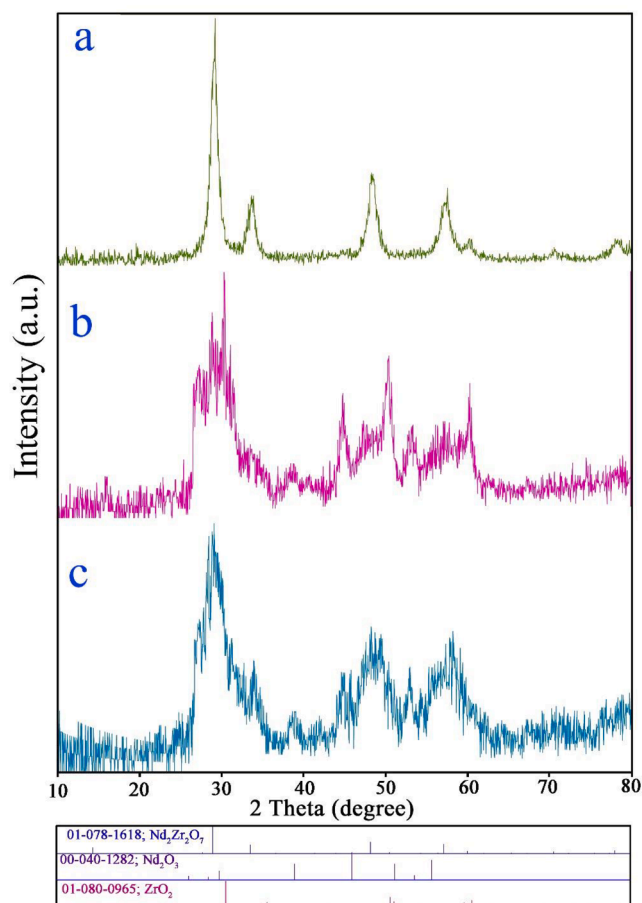


Fig. 2. XRD patterns of (a) net $\text{Nd}_2\text{Zr}_2\text{O}_7$ nanostructure and (b) $\text{Nd}_2\text{Zr}_2\text{O}_7\text{-ZrO}_2$ and (c) $\text{Nd}_2\text{Zr}_2\text{O}_7\text{-Nd}_2\text{O}_3$ nanocomposites fabricated with the help of *Morus nigra* extract via sonochemical pathway.

continued for 10 min. Created precipitate was subsequently rinsed (with ethanol and water) and air-dried. To fabricate $\text{Nd}_2\text{Zr}_2\text{O}_7$ nanostructure, the residue was heated (at 650°C within 90 min in a furnace). In order to create $\text{Nd}_2\text{O}_3\text{-Nd}_2\text{Zr}_2\text{O}_7$ and $\text{ZrO}_2\text{-Nd}_2\text{Zr}_2\text{O}_7$ nanocomposites, 1:2 and 2:1 M ratios of Zr:Nd have been applied, under the conditions mentioned above. Experimental details are visible in Table 1.

2.3. Evaluation of catalytic performance

The performance of the samples was assessed utilizing an integral catalytic reactor illustrated in Fig. 1 [40]. In short, the inlet gas comprise a admixture with nitric oxide (30 ppm), nitrogen dioxide (460 ppm), oxygen (2.5 vol%), C_3H_8 (1000 ppm and also Argon gas (balance). The mentioned composition enters a flow meter set at $300\text{ cm}^3/\text{min}$ (with atmospheric pressure) and afterward is preheated and also steered into an integral reactor comprising 500 mg catalyst. The furnace is responsible for heating the reactor that its diameter is $\frac{1}{2}$ inch. Reactor temperature is regulated in the range of $150\text{--}500^\circ\text{C}$. For measurement of quantity of nitric oxide, nitrogen dioxide, carbon monoxide and O_2 at the outlet of reactor, a KANE 940 analyzer which detects them is utilized. Besides, a gas chromatography (SHIMADZU model 2010 plus) is employed for determining of nitrous oxide quantity in effluent. More data can be found in the previous literature [40].

3. Results and discussion

This paper offered novel framework and easy path to fabricate $\text{Nd}_2\text{Zr}_2\text{O}_7$ nanostructures with the help of ultrasonic approach. The

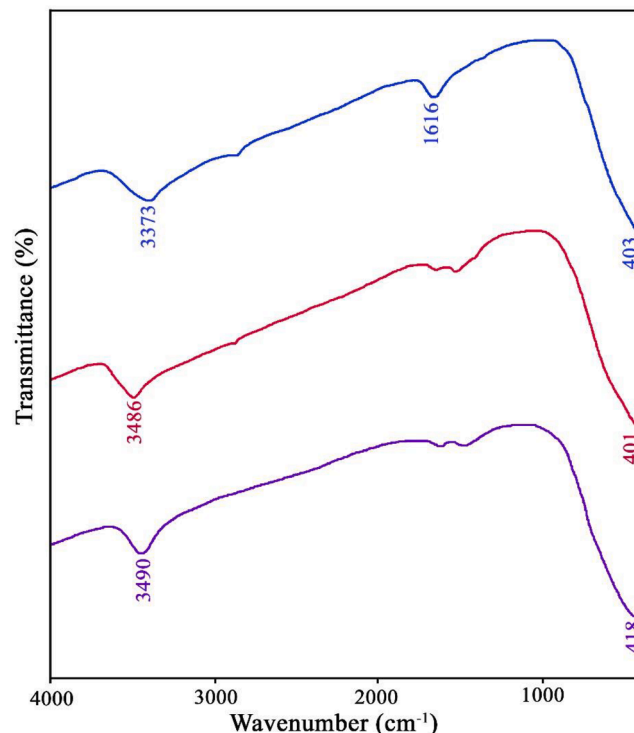


Fig. 3. FT-IR spectra of (a) net $\text{Nd}_2\text{Zr}_2\text{O}_7$ nanostructure and (b) $\text{Nd}_2\text{Zr}_2\text{O}_7\text{-ZrO}_2$ and (c) $\text{Nd}_2\text{Zr}_2\text{O}_7\text{-Nd}_2\text{O}_3$ nanocomposites fabricated with the help of *Morus nigra* extract via sonochemical pathway.

study demonstrates the first try on checking the role of *Morus nigra* extract, as an eco-friendly kind of capping agent, in the sonochemical synthesis of $\text{Nd}_2\text{Zr}_2\text{O}_7$ nanostructures. *Morus nigra* extract has been utilized as a new kind of capping agent because it comprises high quantity of anthocyanins. In addition, the nanostructured $\text{Nd}_2\text{Zr}_2\text{O}_7\text{-ZrO}_2$ and $\text{Nd}_2\text{Zr}_2\text{O}_7\text{-Nd}_2\text{O}_3$ have been fabricated with the help of *Morus nigra* extract via sonochemical pathway, to check the possibility of coupling ZrO_2 or Nd_2O_3 into neodymium zirconate and its effect on shape, dimension and activity.

3.1. Structural determination and purity

The crystal structures of net $\text{Nd}_2\text{Zr}_2\text{O}_7$ nanostructure and $\text{Nd}_2\text{Zr}_2\text{O}_7\text{-ZrO}_2$ and $\text{Nd}_2\text{Zr}_2\text{O}_7\text{-Nd}_2\text{O}_3$ nanocomposites are given in Fig. 2. The intense peaks visible in XRD data are indicative of the crystalline nature of the compounds. XRD pattern of the net $\text{Nd}_2\text{Zr}_2\text{O}_7$ nanostructure exhibits signals that fit well to cubic phase neodymium zirconium oxide (JCPDS No. 78-1618). When 1:2 and 2:1 M ratios of Zr:Nd are applied in the experiment conditions, the nanocomposite samples can be created. It is visible that in the case of $\text{Nd}_2\text{Zr}_2\text{O}_7\text{-ZrO}_2$ nanocomposite, the diffraction signals corresponding to $\text{Nd}_2\text{Zr}_2\text{O}_7$ and tetragonal zirconium oxide (JCPDS No. 80-0965) seen, signifying the incorporation of ZrO_2 over $\text{Nd}_2\text{Zr}_2\text{O}_7$ (see Fig. 2b). Further, $\text{Nd}_2\text{Zr}_2\text{O}_7\text{-Nd}_2\text{O}_3$ nanocomposite denotes diffraction signals corresponding to hexagonal neodymium oxide (JCPDS No. 40-1282) and $\text{Nd}_2\text{Zr}_2\text{O}_7$, implying coupling of both oxides during the fabrication stage (see Fig. 2c). The above-mentioned findings suggest that the process of fabrication nanocomposite does not alter the crystalline structure neodymium zirconium oxide. No other crystalline impurities can be visible, signifying purity of all three samples. The mean crystallite diameters for $\text{Nd}_2\text{Zr}_2\text{O}_7$ -based nanostructure samples have been estimated with Scherer equation (see Table 1).

FT-IR data further verify the formation of $\text{Nd}_2\text{Zr}_2\text{O}_7$ -based nanostructures and their chemical purity. FT-IR data of the net $\text{Nd}_2\text{Zr}_2\text{O}_7$ nanostructure, $\text{Nd}_2\text{Zr}_2\text{O}_7\text{-ZrO}_2$ and $\text{Nd}_2\text{Zr}_2\text{O}_7\text{-Nd}_2\text{O}_3$ nanocomposites (samples 1–3) are visible in Fig. 3a–c. The intensive signals nearly 403,

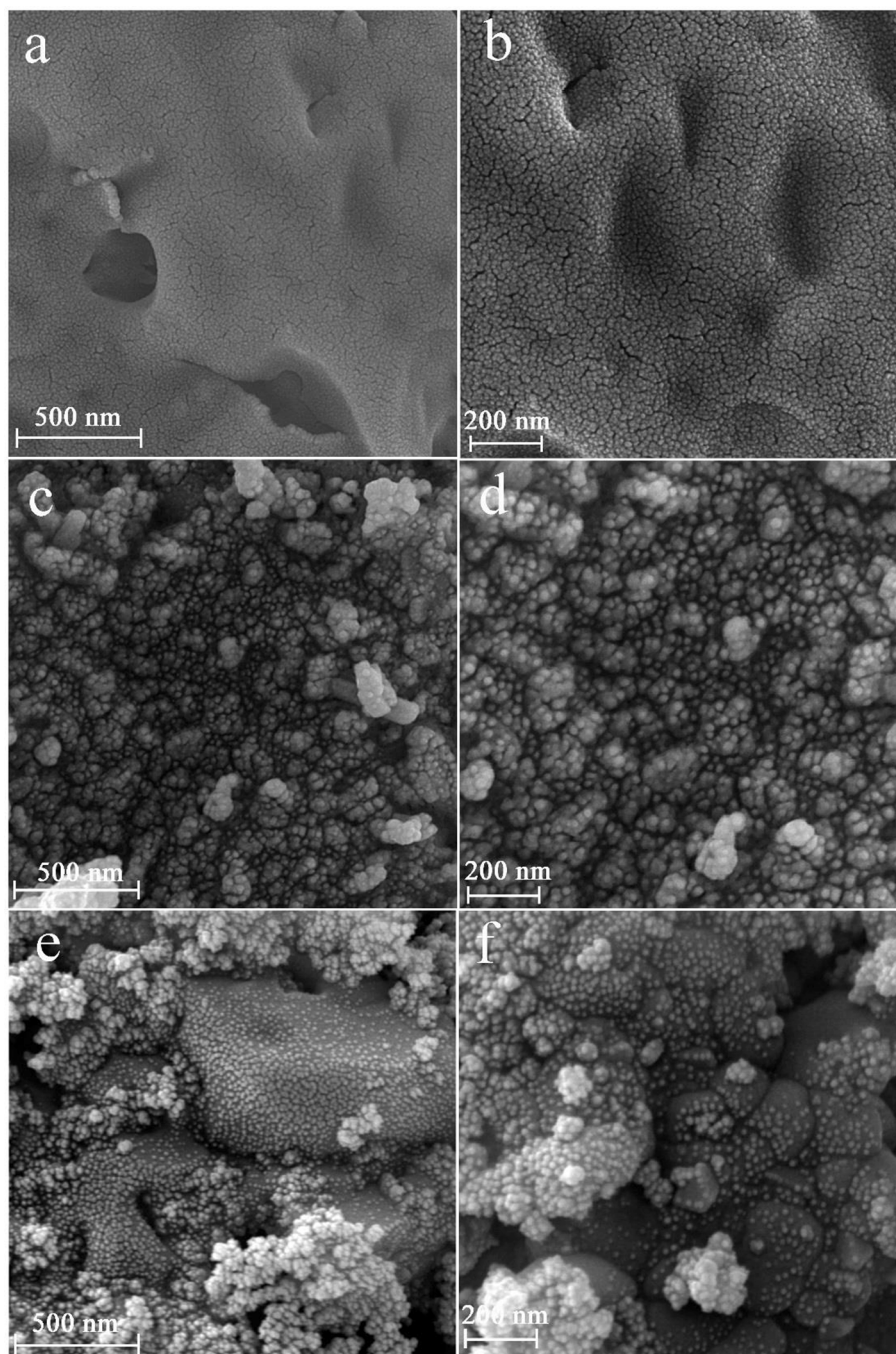


Fig. 4. FESEM images of (a and b) net $\text{Nd}_2\text{Zr}_2\text{O}_7$ nanostructure and (c and d) $\text{Nd}_2\text{Zr}_2\text{O}_7\text{-ZrO}_2$ and (e and f) $\text{Nd}_2\text{Zr}_2\text{O}_7\text{-Nd}_2\text{O}_3$ nanocomposites fabricated with the help of *Morus nigra* extract via sonochemical pathway.

401 and 418 cm^{-1} appeared in FT-IR data of the net $\text{Nd}_2\text{Zr}_2\text{O}_7$ nanostructure, $\text{Nd}_2\text{Zr}_2\text{O}_7\text{-ZrO}_2$ and $\text{Nd}_2\text{Zr}_2\text{O}_7\text{-Nd}_2\text{O}_3$ nanocomposites, correspondingly, were ascribable to the metal-oxygen stretching vibrations [17,41,42]. Besides, signals near 3373 , 1616 , 3486 and 3490 cm^{-1} in FT-IR data of the samples 1–3, correspondingly, are indicative of adsorbed H_2O molecules [43].

3.2. Morphological observations

Morphological aspects of net $\text{Nd}_2\text{Zr}_2\text{O}_7$ nanostructure and $\text{Nd}_2\text{Zr}_2\text{O}_7\text{-ZrO}_2$ and $\text{Nd}_2\text{Zr}_2\text{O}_7\text{-Nd}_2\text{O}_3$ nanocomposites have been checked with FESEM and outcomes are given in Fig. 4. Various morphologies can be visible in the case of three samples. The homogenous nanoparticles are

visible in the case of net $\text{Nd}_2\text{Zr}_2\text{O}_7$ (Fig. 4a and b), and the structure of $\text{Nd}_2\text{Zr}_2\text{O}_7\text{-ZrO}_2$ with a nanobundle-like shape is illustrated in Fig. 4c and d. The morphology for $\text{Nd}_2\text{Zr}_2\text{O}_7\text{-Nd}_2\text{O}_3$ is irregular and agglomerated micro/nanobundle-like (Fig. 4e and f). The outcomes illustrate that the morphology of $\text{Nd}_2\text{Zr}_2\text{O}_7$ is different before and after introduction of ZrO_2 or Nd_2O_3 . Thus, ZrO_2 or Nd_2O_3 can alter the morphology of $\text{Nd}_2\text{Zr}_2\text{O}_7$. All the above samples were fabricated with the help of *Morus nigra* extract. *Morus nigra* extract has been utilized as a new kind of capping agent because it comprises high quantity of anthocyanins that may cause to the convenient steric hindrance effect in sonochemical synthesis phase. The anthocyanins can play a helpful role in adjusting particle size.

TEM data further verify the formation of $\text{Nd}_2\text{Zr}_2\text{O}_7$ -based

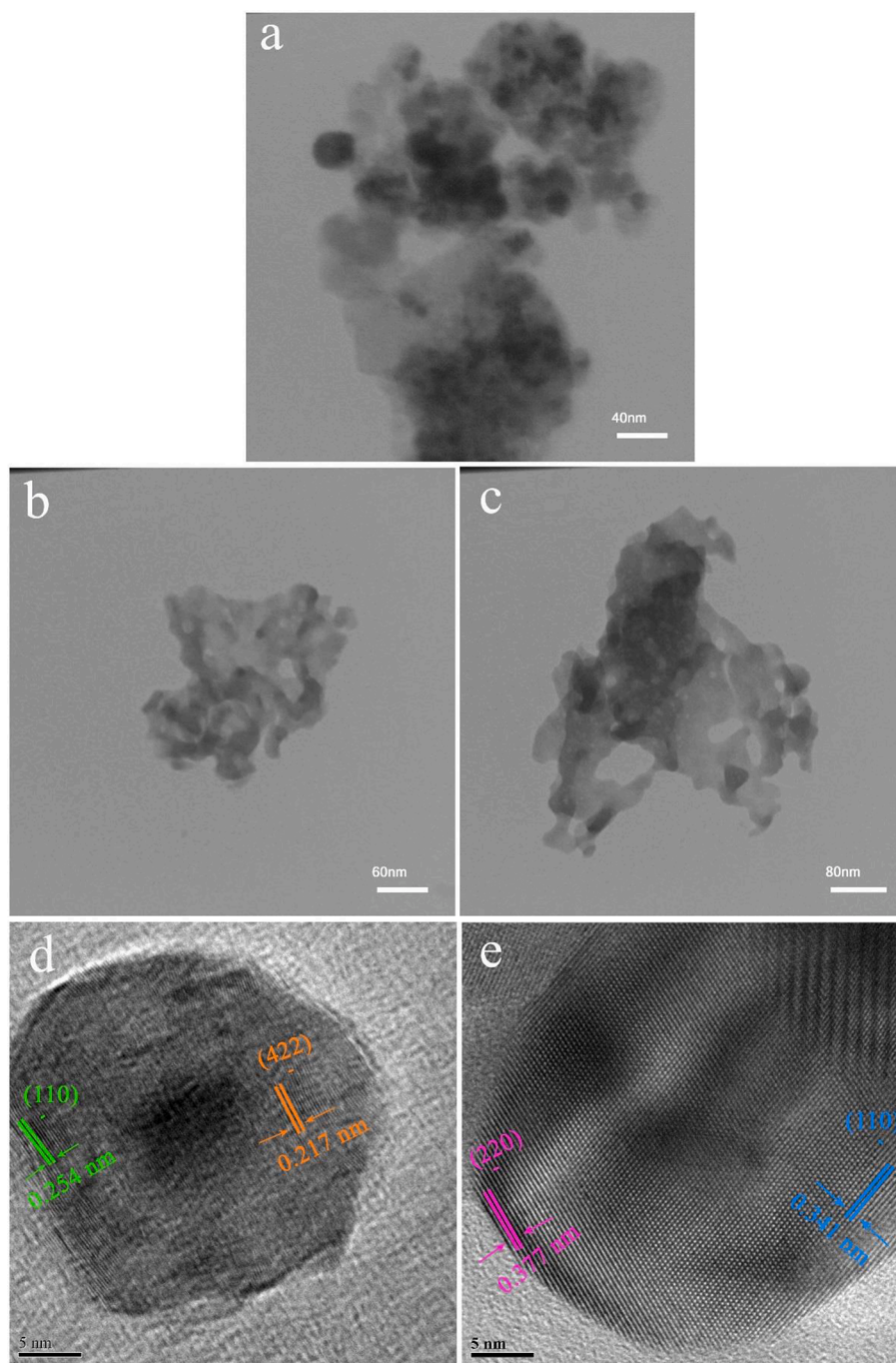


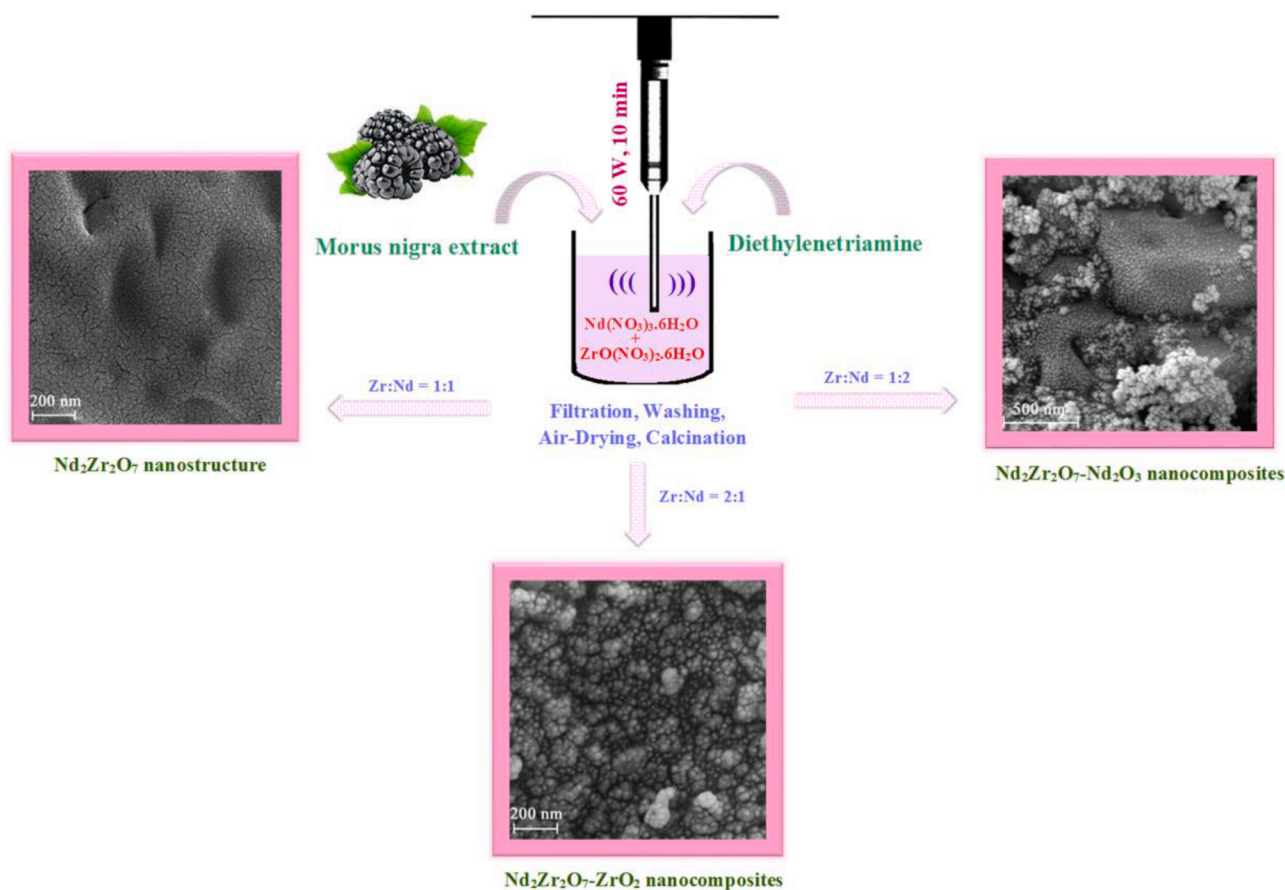
Fig. 5. TEM images of (a) net $\text{Nd}_2\text{Zr}_2\text{O}_7$ nanostructure and (b) $\text{Nd}_2\text{Zr}_2\text{O}_7\text{-ZrO}_2$ and (c) $\text{Nd}_2\text{Zr}_2\text{O}_7\text{-Nd}_2\text{O}_3$ nanocomposites and HRTEM images of (d) $\text{Nd}_2\text{Zr}_2\text{O}_7\text{-ZrO}_2$ and (e) $\text{Nd}_2\text{Zr}_2\text{O}_7\text{-Nd}_2\text{O}_3$ nanocomposites.

nanostructures (see Fig. 5). The sphere-shaped nanoparticles of $\text{Nd}_2\text{Zr}_2\text{O}_7$ are visible in Fig. 5a. TEM data of $\text{Nd}_2\text{Zr}_2\text{O}_7\text{-ZrO}_2$ and $\text{Nd}_2\text{Zr}_2\text{O}_7\text{-Nd}_2\text{O}_3$ nanocomposites (samples 2 and 3) are given in Fig. 5b and c. In agreement with FESEM outcomes, TEM data display the presence of agglomerated nanoparticles. The nanobundle-like morphology of $\text{Nd}_2\text{Zr}_2\text{O}_7\text{-ZrO}_2$ sample is visible in Fig. 5b. $\text{Nd}_2\text{Zr}_2\text{O}_7\text{-Nd}_2\text{O}_3$ sample illustrates the irregular and agglomerated micro/nanobundle-like structure assembled by nanoparticles (see Fig. 5c). HRTEM data of both the nanocomposite samples denote the lattice fringes (Fig. 5d and e). The lattice fringes of $\text{Nd}_2\text{Zr}_2\text{O}_7\text{-ZrO}_2$ sample demonstrate the interplanar distances of cubic neodymium zirconium oxide and tetragonal zirconium oxide. The observed interplanar distance (d) of 0.25 nm correspond to 1 1 0 planes of tetragonal zirconium oxide

(JCPDS No. 80-0965), and the measured 0.21 nm agrees with the d of 4 2 2 planes of cubic neodymium zirconium oxide (JCPDS No. 78-1618). The corresponding data of $\text{Nd}_2\text{Zr}_2\text{O}_7\text{-Nd}_2\text{O}_3$ sample illustrate the interplanar distances of the 2 2 0 planes of cubic neodymium zirconium oxide (0.37 nm) and the 1 1 0 planes of hexagonal neodymium oxide (0.34 nm) lattices. The above-mentioned findings as well as XRD and FTIR data represent that samples 2 and 3, are desirous compounds, namely, $\text{Nd}_2\text{Zr}_2\text{O}_7\text{-ZrO}_2$ and $\text{Nd}_2\text{Zr}_2\text{O}_7\text{-Nd}_2\text{O}_3$ nanocomposites.

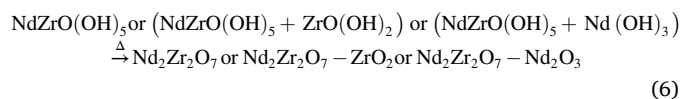
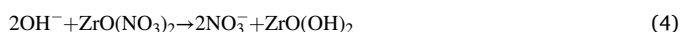
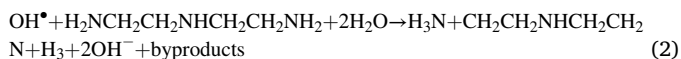
3.3. Sonication effect and formation mechanism

As mentioned above, $\text{Nd}_2\text{Zr}_2\text{O}_7$ -based nanostructures were fabricated through a simple and eco-friendly sonochemical pathway with the



Scheme 1. Schematic diagram for creation $\text{Nd}_2\text{Zr}_2\text{O}_7$ -based nanostructures.

help of *Morus nigra* extract as a new kind of capping agent. Cavitation resulting from ultrasonic waves can create appropriate and particular structures in nano dimension and homogeneous trend. Extensive usage of ultrasonic approach for making the nanoscale compounds can be for its ease, fastness and low cost as well as its environmental friendliness [18–21]. Multiple bubbles are created within the sonochemical path. After growth stage, these bubbles destructed because of the shake waves. The energy release by bubbles destruction can be reason to drive the chemical reactions to form our products [24,25]. Further, the anthocyanins in *Morus nigra* extract can play a helpful role in adjusting particle size. The key and possible reactions for the sonochemical formation of $\text{Nd}_2\text{Zr}_2\text{O}_7$ -based nanostructures with the help of dien may be as [44,45]:



The decomposition of O–H bond in water augments the quantity of OH radical species. The generated OH radicals can be reason for creation of the OH^- ions (Eq. (2)), which can play a key and helpful role in

formation of $\text{Nd}_2\text{Zr}_2\text{O}_7$ -based nanostructures. Subsequently, reaction of ZrO^{2-} and Nd^{3+} with OH^- brings to creation of metal hydroxide and formation of $\text{Nd}_2\text{Zr}_2\text{O}_7$ -based nanostructures performed as illustrated in Eq. (5), 6 (see Scheme 1).

3.4. Surface characteristics

Catalytic performance of the nanoscale compounds can be dependent to the surface characteristics of them. These characteristics (surface area and porosity) are checked via nitrogen adsorption process. The adsorption–desorption isotherms of net $\text{Nd}_2\text{Zr}_2\text{O}_7$ nanostructure and $\text{Nd}_2\text{Zr}_2\text{O}_7$ - ZrO_2 nanocomposite are compared in Fig. 6. Based on the outcomes, both samples display the mesoporous structure. Further, the specific surface areas of net $\text{Nd}_2\text{Zr}_2\text{O}_7$ nanostructure and $\text{Nd}_2\text{Zr}_2\text{O}_7$ - ZrO_2 nanocomposite were 26.435 and 32.637 m^2/g , correspondingly. Table 2 gives the textural features of the $\text{Nd}_2\text{Zr}_2\text{O}_7$ -based nanostructures. It is visible that the surface area of $\text{Nd}_2\text{Zr}_2\text{O}_7$ - ZrO_2 nanocomposite is greater than that of net $\text{Nd}_2\text{Zr}_2\text{O}_7$. The mesoporous structures and convenient surface area of the $\text{Nd}_2\text{Zr}_2\text{O}_7$ -based nanostructures can be conducive to the possibility of highly efficient catalytic performance.

3.5. Catalytic activity

According to GC analysis, nitrous oxide was absent in the outlet streams. Hence, nitrogen in the product might be obtained via mass balance of nitric oxide and nitrogen dioxide which are traceable with Kane 940 gas analyzer. To examine the role of synthesis pathway, the activity of $\text{Nd}_2\text{Zr}_2\text{O}_7$ samples produced by two different pathways (sonochemical and combustion) on propane-SCR- NO_x is compared at a GHSV (gas hourly space velocity) of 47048 h^{-1} (see Fig. 7). It is visible

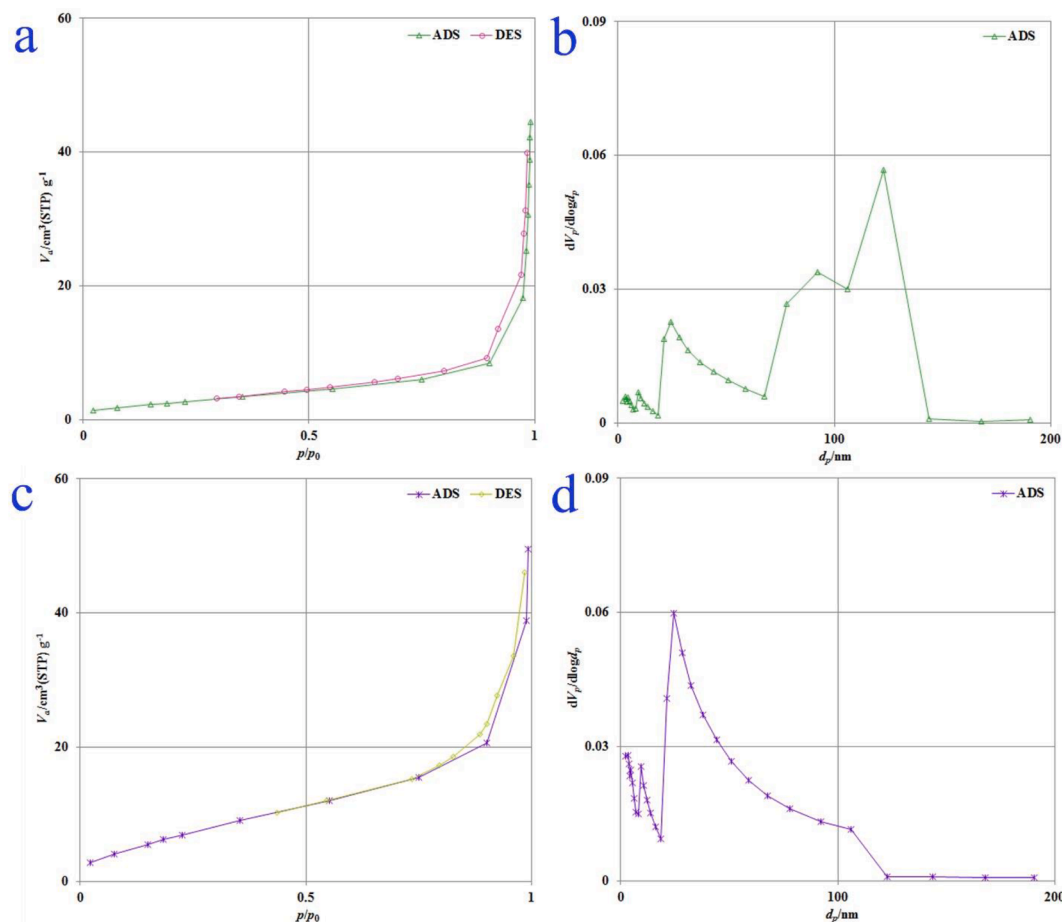


Fig. 6. N_2 adsorption/desorption isotherms (a and c) and pore size distribution curves (b and d) of net $\text{Nd}_2\text{Zr}_2\text{O}_7$ nanostructure and $\text{Nd}_2\text{Zr}_2\text{O}_7\text{-ZrO}_2$ nanocomposites, correspondingly.

that by enhancement of temperature, NO_x conversion rate to nitrogen is grown and afterward is reduced after 400 °C for both of $\text{Nd}_2\text{Zr}_2\text{O}_7$ nanostructure samples. Both of nanostructures may manifest maximum conversion at 400 °C since, conversion of NO_x to nitrogen for $\text{Nd}_2\text{Zr}_2\text{O}_7$ (fabricated by sonochemical approach) is 64% and for $\text{Nd}_2\text{Zr}_2\text{O}_7$ (sample.1 in Ref. [38] fabricated by combustion approach) is 56%. From XRD data (see Table 1), it is visible that the crystallite size of $\text{Nd}_2\text{Zr}_2\text{O}_7$ nanostructure (fabricated by sonochemical approach) is 11 nm and for $\text{Nd}_2\text{Zr}_2\text{O}_7$ (fabricated by combustion approach) is 20 nm. Thus, $\text{Nd}_2\text{Zr}_2\text{O}_7$ nanostructure (fabricated by sonochemical approach) has the crystallite size smaller than the other sample. Besides, FESEM findings demonstrate that particle size of $\text{Nd}_2\text{Zr}_2\text{O}_7$ nanostructure (fabricated by sonochemical approach) is smaller. Also, this nanostructure possesses better uniformity. It is worthy to note that the enhancement of surface area from 11.504 for $\text{Nd}_2\text{Zr}_2\text{O}_7$ (fabricated by combustion approach) to 26.435 m^2g^{-1} for the $\text{Nd}_2\text{Zr}_2\text{O}_7$ nanostructure (fabricated by sonochemical approach) also may possess a positive effect upon the catalytic performance. Thus, very convenient surface area as well as smaller and also more homogeneous nanoparticles can be reasons for more proper conversion of $\text{Nd}_2\text{Zr}_2\text{O}_7$ nanostructure (fabricated by sonochemical approach).

In following, the effect of adding Nd_2O_3 and ZrO_2 to $\text{Nd}_2\text{Zr}_2\text{O}_7$ on the performance of NO_x conversion to N_2 was checked. Fig. 8 exhibits plots of the total NO_x conversion into nitrogen versus reaction temperature for $\text{Nd}_2\text{Zr}_2\text{O}_7$ -based ceramic nanostructure materials at a GHSV of 47048 h^{-1} . A similar trend between the performances of the various samples is seeable. In the case of all samples, there is a maximum conversion in 400 °C. Regarding the maximum conversion temperature, it is visible that $\text{Nd}_2\text{Zr}_2\text{O}_7\text{-Nd}_2\text{O}_3$ possesses the least rate of conversion (52%). Net $\text{Nd}_2\text{Zr}_2\text{O}_7$ displays a maximal conversion of 64%. This is while $\text{Nd}_2\text{Zr}_2\text{O}_7\text{-ZrO}_2$

Table 2

Summary of surface features for $\text{Nd}_2\text{Zr}_2\text{O}_7$ -based nanostructure materials.

| Sample | BET area (m^2g^{-1}) | Pore volume (cm^3g^{-1}) | Pore diameter (nm) |
|--|--|--|--------------------|
| $\text{Nd}_2\text{Zr}_2\text{O}_7$ | 26.435 | 0.1527 | 18.216 |
| $\text{Nd}_2\text{Zr}_2\text{O}_7\text{-ZrO}_2$ | 32.637 | 0.1843 | 15.177 |
| $\text{Nd}_2\text{Zr}_2\text{O}_7\text{-Nd}_2\text{O}_3$ | 6.423 | 0.0624 | 36.541 |

ZrO_2 illustrates a very appreciable maximum conversion of 70%. It would be informative and helpful to consider the change in the nitrogen adsorption features of the samples. Fig. 6a and c illustrate the nitrogen adsorption isotherms of $\text{Nd}_2\text{Zr}_2\text{O}_7$ and $\text{Nd}_2\text{Zr}_2\text{O}_7\text{-ZrO}_2$ respectively. It is plainly perceived that the adsorption capacity enhances in sample of $\text{Nd}_2\text{Zr}_2\text{O}_7\text{-ZrO}_2$. This phenomenon is in compliance with the creation of an observed hysteresis in the adsorption/desorption isotherms at upper range of volume so that pore volume increases from 0.1527 to 0.1843 cm^3g^{-1} . This is accompanied with an enhancement of the specific surface area from 26.435 to 32.637 m^2g^{-1} . It is valuable to mention that, the increase of surface area (see Table 2) influence positively the catalytic activity. It can be state that, the remarkable increment of surface area in the case of $\text{Nd}_2\text{Zr}_2\text{O}_7\text{-ZrO}_2$ (from 6.423 to 32.637 m^2g^{-1}) and also enhancement of pore volume (from 0.0624 to 0.1843 cm^3g^{-1}) positively affect the catalytic yield. Moreover, FESEM findings illustrate that $\text{Nd}_2\text{Zr}_2\text{O}_7\text{-ZrO}_2$ nanocomposite has smaller and also more homogeneous nanoparticles. It is worthy to note that, from XRD outcomes, the crystallinity of the $\text{Nd}_2\text{Zr}_2\text{O}_7\text{-Nd}_2\text{O}_3$ is lower than the rest so that as

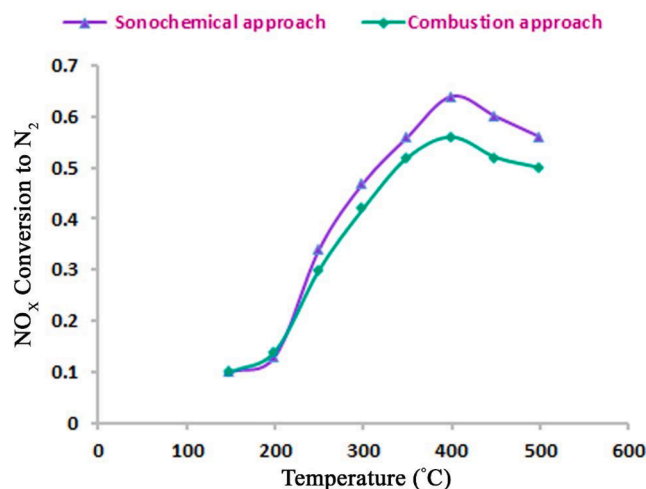


Fig. 7. The role of the reaction temperature and kind of nanostructure (produced by two different pathways) on the conversion of NO_x (NO + NO₂) into N₂ in the range of 150–500 °C.

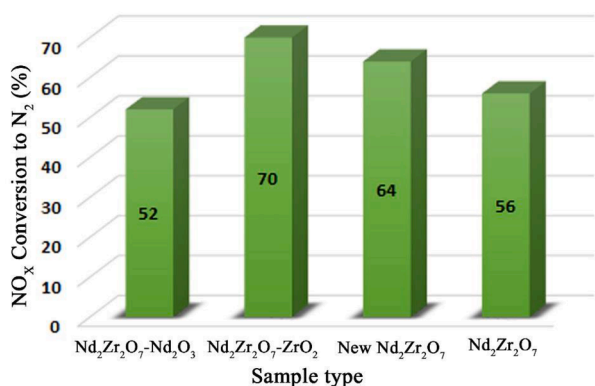
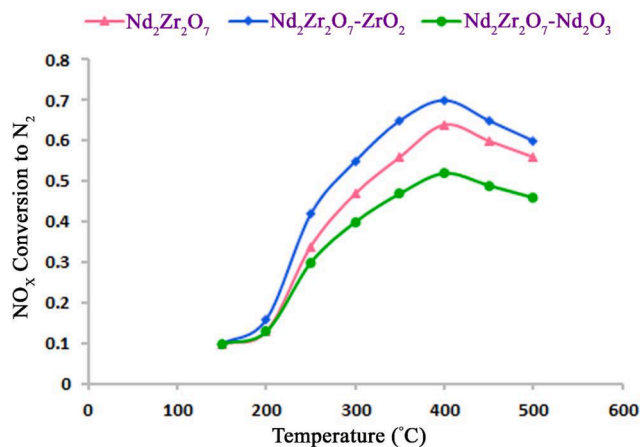


Fig. 8. Plots of total conversion of NO_x (NO + NO₂) into N₂ versus reaction temperature for Nd₂Zr₂O₇-based ceramic nanostructure materials in the range of 150–500 °C.

demonstrated at previous works [46], decrement of crystallinity may lead to fall of performance. Summing up, very appropriate surface area as well as having fine and also homogeneous nanoparticles can be reasons for more favorable conversion of Nd₂Zr₂O₇-ZrO₂ nanocomposite.

Fig. 9 denotes plots of the outlet CO concentration of reactor versus reaction temperature for Nd₂Zr₂O₇-based ceramic nanostructure materials. It is visible that for Nd₂Zr₂O₇-ZrO₂ nanocomposite, quantity of CO production is minimum (30 ppm at 500 °C) in comparison with the rest.

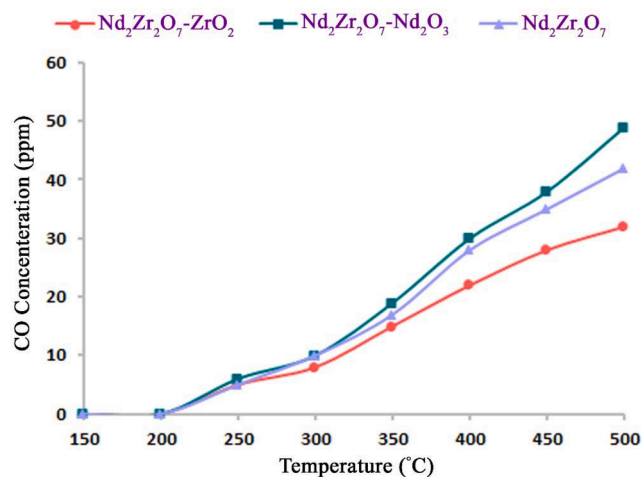


Fig. 9. Plots of the outlet CO concentration of reactor versus reaction temperature for Nd₂Zr₂O₇-based ceramic nanostructure materials.

Recall, creation of CO as an unfavorable product during NO_x abatement by hydrocarbons like C₃H₈ is unavoidable. This occurrence may be related to the unselective combustion of C₃H₈ at greater temperatures, as stated in previous works [38,39]. Further, reaction of CO creation can be activated within the nanostructure channel and do not exclusively take place in the gas phase. Further data on this topic can be found in the previous literature [37].

4. Conclusions

In summary, a simple and swift pathway was selected to fabricate beneficial active materials, which can be employed on propane-SCR-NO_x. Nd₂Zr₂O₇ nanostructures and nanocomposites were sonochemically fabricated with the help of Morus nigra extract as a new kind of capping agent. For the first time, the performance of Nd₂Zr₂O₇-based ceramic nanostructure materials has been compared on propane-SCR-NO_x. Outcomes revealed the successful fabrication of Nd₂Zr₂O₇ nanostructures and nanocomposites applying Morus nigra extract through sonochemical pathway. It is demonstrated that ultrasound irradiation can play a helpful role in formation of Nd₂Zr₂O₇-based nanostructures. Further, the fabricated Nd₂Zr₂O₇-based ceramic nanostructure materials

can be applied as potential nanocatalysts with appropriate performance for propane-SCR-NO_x. The synthesis way facilitated large scale production as a result of its easiness, fastness and low cost as well as its environmental friendliness. Further, these Nd₂Zr₂O₇-based ceramic nanostructure materials might find substantial usages in relevant fields.

CRedit authorship contribution statement

Sahar Zinatloo-Ajabshir: Formal analysis, Investigation, Data curation, Conceptualization, Methodology, Supervision, Project administration, Validation, Writing - review & editing, Writing - original draft, Resources. **Naser Ghasemian:** Formal analysis, Investigation, Data curation, Validation, Writing - original draft. **Mehdi Mousavi-Kamazani:** Software, Writing - review & editing, Resources, Visualization. **Masoud Salavati-Niasari:** Formal analysis, Investigation, Data curation, Writing - review & editing.

Declaration of Competing Interest

The authors declare that they have no known competing financial interests or personal relationships that could have appeared to influence the work reported in this paper.

Acknowledgements

Authors are grateful to the council of University of Bonab for supporting this work.

References

- Y. Chen, C. Shen, J. Wang, G. Xiao, G. Luo, Green synthesis of Ag-TiO₂ supported on porous glass with enhanced photocatalytic performance for oxidative desulfurization and removal of dyes under visible light, *ACS Sustainable Chem. Eng.* 6 (2018) 13276–13286.
- S. Zinatloo-Ajabshir, S. Zinatloo-Ajabshir, Preparation and characterization of Curcumin niosomal nanoparticles via a simple and eco-friendly route, *J. Nanostruct.* 9 (2019) 784–790.
- Y. Si, Z. Guo, Superhydrophobic nanocoatings: from materials to fabrications and to applications, *Nanoscale* 7 (2015) 5922–5946.
- S. Mortazavi-Derazkola, S. Zinatloo-Ajabshir, M. Salavati-Niasari, Facile hydrothermal and novel preparation of nanostructured Ho₂O₃ for photodegradation of eriochrome black T dye as water pollutant, *Adv. Powder Technol.* 28 (2017) 747–754.
- B. Saruhan, P. Francois, K. Fritscher, U. Schulz, EB-PVD processing of pyrochlore-structured La₂Zr₂O₇-based TBCs, *Surf. Coat. Technol.* 182 (2004) 175–183.
- Y. Tong, L. Lu, X. Yang, X. Wang, Characterization and their photocatalytic properties of Ln₂Zr₂O₇ (Ln=La, Nd, Sm, Dy, Er) nanocrystals by stearic acid method, *Solid State Sci.* 10 (2008) 1379–1383.
- S. Zinatloo-Ajabshir, M. Salavati-Niasari, Facile synthesis of nanocrystalline neodymium zirconate for highly efficient photodegradation of organic dyes, *J. Mol. Liq.* 243 (2017) 219–226.
- X. Fang, L. Xia, L. Peng, Y. Luo, J. Xu, L. Xu, X. Xu, W. Liu, R. Zheng, X. Wang, Ln₂Zr₂O₇ compounds (Ln = La, Pr, Sm, Y) with varied rare earth A sites for low temperature oxidative coupling of methane, *Chin. Chem. Lett.* 30 (2019) 1141–1146.
- Y. Tong, Y. Wang, Z. Yu, X. Wang, X. Yang, L. Lu, Preparation and characterization of pyrochlore La₂Zr₂O₇ nanocrystals by stearic acid method, *Mater. Lett.* 62 (2008) 889–891.
- X. Zhang, X. Fang, X. Feng, X. Li, W. Liu, X. Xu, N. Zhang, Z. Gao, X. Wang, W. Zhou, Ni/Ln₂Zr₂O₇ (Ln = La, Pr, Sm and Y) catalysts for methane steam reforming: the effects of A site replacement, *Catal. Sci. Technol.* 7 (2017) 2729–2743.
- S. Zinatloo-Ajabshir, Z. Zinatloo-Ajabshir, M. Salavati-Niasari, S. Bagheri, S.B. A. Hamid, Facile preparation of Nd₂Zr₂O₇-ZrO₂ nanocomposites as an effective photocatalyst via a new route, *J. Energy Chem.* 26 (2017) 315–323.
- O. Fabrichnaya, R. Wulf, M.J. Krieger, G. Savinykh, M. Dopita, J. Seidel, H.C. Heitz, O. Nashed, U. Gross, H.J. Seifert, Thermophysical properties of pyrochlore and fluorite phases in the Ln₂Zr₂O₇-Y₂O₃ systems (Ln=La, Nd, Sm): 2. Comparison of conventionally sintered and SPS samples in the systems Nd₂Zr₂O₇-Y₂O₃ and Sm₂Zr₂O₇-Y₂O₃, *J. Alloys Compounds* 625 (2015) 200–207.
- V.V. Popov, A.P. Menushenkov, A.A. Ivanov, B.R. Gaynanov, A.A. Yastrebsev, F. d'Acapito, A. Puri, G.R. Castro, I.V. Shchetinin, M.V. Zheleznyi, Y.V. Zubavichus, K.V. Ponkratov, Comparative analysis of long- and short-range structures features in titanates Ln₂Ti₂O₇ and zirconates Ln₂Zr₂O₇ (Ln = Gd, Tb, Dy) upon the crystallization process, *J. Phys. Chem. Solids* 130 (2019) 144–153.
- M. Ciomaga Hatnean, M.R. Lees, G. Balakrishnan, Growth of single-crystals of rare-earth zirconate pyrochlores, Ln₂Zr₂O₇ (with Ln=La, Nd, Sm, and Gd) by the floating zone technique, *J. Cryst. Growth* 418 (2015) 1–6.
- S. Zinatloo-Ajabshir, M. Salavati-Niasari, A. Sobhani, Z. Zinatloo-Ajabshir, Rare earth zirconate nanostructures: recent development on preparation and photocatalytic applications, *J. Alloy. Compd.* (2018).
- Y.-H. Chou, N. Hondow, C.I. Thomas, R. Mitchell, R. Brydson, R.E. Douthwaite, Microwave plasma synthesis of lanthanide zirconates from microwave transparent oxides, *Dalton Trans.* 41 (2012) 2472–2476.
- S. Zinatloo-Ajabshir, M. Salavati-Niasari, Z. Zinatloo-Ajabshir, Nd₂Zr₂O₇-Nd₂O₃ nanocomposites: new facile synthesis, characterization and investigation of photocatalytic behaviour, *Mater. Lett.* 180 (2016) 27–30.
- S. Gholamrezaei, M. Ghanbari, O. Amiri, M. Salavati-Niasari, L.K. Foong, BaMnO₃ nanostructures: simple ultrasonic fabrication and novel catalytic agent toward oxygen evolution of water splitting reaction, *Ultrason. Sonochem.* 61 (2020) 104829.
- S. Zinatloo-Ajabshir, S. Mortazavi-Derazkola, M. Salavati-Niasari, Nd₂O₃-SiO₂ nanocomposites: a simple sonochemical preparation, characterization and photocatalytic activity, *Ultrason. Sonochem.* 42 (2018) 171–182.
- Y. Qin, L. Xue, Y. Hu, C. Qiu, Z. Jin, X. Xu, J. Wang, Green fabrication and characterization of debranched starch nanoparticles via ultrasonication combined with recrystallization, *Ultrason. Sonochem.* 66 (2020) 105074.
- S. Zinatloo-Ajabshir, S. Mortazavi-Derazkola, M. Salavati-Niasari, Sonochemical synthesis, characterization and photodegradation of organic pollutant over Nd₂O₃ nanostructures prepared via a new simple route, *Sep. Purif. Technol.* 178 (2017) 138–146.
- M. Salavati-Niasari, M. Esmaeili-Zare, A. Sobhani, Synthesis and characterisation of cadmium selenide nanostructures by simple sonochemical method, *Micro Nano Lett.* 7 (2012) 831–834.
- M. Salavati-Niasari, M. Esmaeili-Zare, A. Sobhani, Cubic HgSe nanoparticles: sonochemical synthesis and characterisation, *Micro Nano Lett.* 7 (2012) 1300–1304.
- R. Monsef, M. Ghiyasiyan-Arani, O. Amiri, M. Salavati-Niasari, Sonochemical synthesis, characterization and application of PrVO₄ nanostructures as an effective photocatalyst for discoloration of organic dye contaminants in wastewater, *Ultrason. Sonochem.* 61 (2020) 104822.
- S. Zinatloo-Ajabshir, S. Mortazavi-Derazkola, M. Salavati-Niasari, Simple sonochemical synthesis of Ho₂O₃-SiO₂ nanocomposites as an effective photocatalyst for degradation and removal of organic contaminant, *Ultrason. Sonochem.* 39 (2017) 452–460.
- H. Zhang, C. Lu, H. Hou, Y. Ma, S. Yuan, Facile morphology-controlled synthesis of Co₃O₄ nanostructure on carbon cloth and their morphology-dependent pseudocapacitive performances, *J. Alloy. Compd.* 797 (2019) 970–977.
- S. Zinatloo-Ajabshir, M.S. Morassaei, O. Amiri, M. Salavati-Niasari, Green synthesis of dysprosium stannate nanoparticles using Ficus carica extract as photocatalyst for the degradation of organic pollutants under visible irradiation, *Ceram. Int.* 46 (2020) 6095–6107.
- J.-Y. Chen, S.-L. Jheng, C.-Y. Chan, H.-Y. Tuan, Morphology controlled synthesis of Pd₂Ge nanostructures and their shape-dependent catalytic properties for hydrogen evolution reaction, *Int. J. Hydrogen Energy* 44 (2019) 12958–12970.
- M.S. Morassaei, S. Zinatloo-Ajabshir, M. Salavati-Niasari, Nd₂Sn₂O₇ nanostructures: new facile Pechini preparation, characterization, and investigation of their photocatalytic degradation of methyl orange dye, *Adv. Powder Technol.* 28 (2017) 697–705.
- B. Zhou, Y. Li, J. Bai, X. Li, F. Li, L. Liu, Controlled synthesis of rh-In₂O₃ nanostructures with different morphologies for efficient photocatalytic degradation of oxytetracycline, *Appl. Surf. Sci.* 464 (2019) 115–124.
- M. Esmaeili-Zare, M. Salavati-Niasari, A. Sobhani, Sonochemical synthesis of HgSe nanoparticles: effect of metal salt, reaction time and reductant agent, *J. Ind. Eng. Chem.* 20 (2014) 3518–3523.
- M. Jafari, A. Sobhani, M. Salavati-Niasari, Effect of preparation conditions on synthesis of Ag₂Se nanoparticles by simple sonochemical method assisted by thiourea, *J. Ind. Eng. Chem.* 20 (2014) 3775–3779.
- P. Sazama, L. Mokrzycki, B. Wichterlova, A. Vondrova, R. Pilar, J. Dedecek, S. Sklenak, E. Tabor, Unprecedented propane-SCR-NO_x activity over template-free synthesized Al-rich Co-BEA* zeolite, *J. Catal.* 332 (2015) 201–211.
- M. Kantcheva, I. Cayirtepe, A. Naydenov, G. Ivanov, FT-IR spectroscopic investigation of the effect of SO₂ on the SCR of NO_x with propene over ZrO₂-Nb₂O₅ catalyst, *Catal. Today* 176 (2011) 437–440.
- M.A. Gómez-García, Y. Zimmermann, V. Pitchon, A. Kiennemann, Multifunctional catalyst for de-NO_x processes: the selective reduction of NO_x by methane, *Catal. Commun.* 8 (2007) 400–404.
- S. Mohan, P. Dinesha, S. Kumar, NO_x reduction behaviour in copper zeolite catalysts for ammonia SCR systems: a review, *Chem. Eng. J.* 384 (2020) 123253.
- N. Ghasemian, C. Falamaki, Zn²⁺, Fe²⁺, Cu²⁺, Mn²⁺, H⁺ ion-exchanged and raw clinoptilolite zeolite catalytic performance in the propane-SCR-NO_x process: a comparative study, *16 (2017) 20160192.*
- S. Zinatloo-Ajabshir, N. Ghasemian, M. Salavati-Niasari, Green synthesis of Ln₂Zr₂O₇ (Ln = Nd, Pr) ceramic nanostructures using extract of green tea via a facile route and their efficient application on propane-selective catalytic reduction of NO_x process, *Ceram. Int.* 46 (2020) 66–73.
- A. Speciale, F. Cimino, A. Saija, R. Canali, F. Virgili, Bioavailability and molecular activities of anthocyanins as modulators of endothelial function, *Genes Nutr.* 9 (2014) 404.

- [40] N. Ghasemian, C. Falamaki, M. Kalbasi, Clinoptilolite zeolite as a potential catalyst for propane-SCR-NOx: performance investigation and kinetic analysis, *Chem. Eng. J.* 236 (2014) 464–470.
- [41] W.E. Klee, G. Weitz, Infrared spectra of ordered and disordered pyrochlore-type compounds in the series RE₂Ti₂O₇, RE₂Zr₂O₇ and RE₂Hf₂O₇, *J. Inorg. Nucl. Chem.* 31 (1969) 2367–2372.
- [42] V.G. Sevast'yanov, E.P. Simonenko, N.P. Simonenko, K.A. Sakharov, N. T. Kuznetsov, Synthesis of finely dispersed La₂Zr₂O₇, La₂Hf₂O₇, Gd₂Zr₂O₇ and Gd₂Hf₂O₇ oxides, *Mendeleev Commun.* 23 (2013) 17–18.
- [43] S. Moshtaghi, S. Zinatloo-Ajabshir, M. Salavati-Niasari, Nanocrystalline barium stannate: facile morphology-controlled preparation, characterization and investigation of optical and photocatalytic properties, *J. Mater. Sci.: Mater. Electron.* 27 (2016) 834–842.
- [44] S. Zinatloo-Ajabshir, S. Mortazavi-Derazkola, M. Salavati-Niasari, Sono-synthesis and characterization of Ho₂O₃ nanostructures via a new precipitation way for photocatalytic degradation improvement of erythrosine, *Int. J. Hydrogen Energy* 42 (2017) 15178–15188.
- [45] S. Zinatloo-Ajabshir, M. Salavati-Niasari, Facile route to synthesize zirconium dioxide (ZrO₂) nanostructures: structural, optical and photocatalytic studies, *J. Mol. Liq.* 216 (2016) 545–551.
- [46] N. Ghasemian, C. Falamaki, M. Kalbasi, M. Khosravi, Enhancement of the catalytic performance of H-clinoptilolite in propane-SCR-NOx process through controlled dealumination, *Chem. Eng. J.* 252 (2014) 112–119.